

# **A strategy for prestack processing of data acquired with crossed-array geometries**

Gijs J.O. Vermeer, *3DSymSam - Geophysical Advice*

## **Abstract**

3D symmetric sampling is based on correct sampling of the minimal data sets (MDSs), which typify the chosen acquisition geometry. The MDSs of all crossed-array geometries, such as orthogonal geometry, have limited extent, unlike the common-offset gathers which are the MDSs of parallel geometry.

Conventional prestack processing suffers from the absence of proper common-offset gathers in the crossed-array geometries. This requires a new approach to prestack processing, which recognises the particular requirements of those geometries. This paper provides a strategy for prestack processing based on the construction of pseudo-minimal data sets (pMDSs), i.e., data sets, which are as nearly as possible MDSs, yet extend across the whole survey area. The strategy assumes 3D symmetric sampling of the input data. The most suitable pMDSs in orthogonal geometry are collections of offset-vector slots (OVS gathers). Each OVS contains data with a limited in-line offset range and a limited cross-line offset range.

Application of OVS gathers is discussed for a number of prestack processes. Even muting can benefit from better insight in the composition of the acquired data; this will lead to a reduction of acquisition footprint by equalising fold for every time slice. The computation of statics can benefit from measuring time shifts in the nearest-neighbour environment offered by OVS gathers, rather than conventional measurements in common-shot gathers or common-midpoint gathers.

AvO measurement in orthogonal geometry is often considered problematic, one of the reasons being that not all offsets occur in each midpoint. As an alternative AvO can be measured in OVSs. At each point, the collection of all overlapping OVSs can be used to get a full picture of AvO in that point. However, the spatial resolution of this measurement is not as good as in a parallel geometry. Finally, a synthesis of recent ideas leads to a new approach to true-amplitude prestack migration, again based on the use of OVS gathers.

## ***Introduction***

3D seismic surveys have become a major tool for mapping the subsurface in hydrocarbon exploration and production. The selection of parameters for those surveys deserves a good deal of attention. On land, and also in seabed acquisition, the positions of sources and receivers are decoupled, allowing a wide variety of different acquisition designs.

To cope with the bewildering number of possibilities for seismic acquisition geometries, various 3D design packages have been developed. For 2D, Anstey (1986) showed, followed by other authors (Ongkiehong and Askin, 1987; Vermeer, 1990) that a regular offset distribution in each CMP is important for an optimum stack response. Most of the 3D design packages tend to extend this insight to 3D. Therefore, they concentrate on analysis of various bin attributes, such as fold, offset distribution, spider diagrams, etc. Because it is felt that a 3D survey should have minimal variation of its bin attributes across the survey area, regularity of those attributes across the survey area is one of the criteria used in the evaluation of a survey design.

The idea of 3D symmetric sampling (Vermeer, 1994, 1998a,b) added some new insights to the design of 3D surveys. Apart from the prescription that source and receiver sampling should be as similar as feasible in all respects, it also introduced the concept of spatial continuity as an important criterion. Spatial continuity can best be defined as the absence of spatial discontinuities, in particular in the spatial attributes of the acquired data. It is important as any discontinuity may give rise to artefacts, especially after migration. In 3D, spatial continuity should extend in the cross-line direction as well as in the in-line direction.

In orthogonal geometry (parallel source lines perpendicular to parallel receiver lines) the largest spatially continuous unit is the cross-spread. It is the collection of all traces, acquired with sources along a single source line and recorded with receivers along a single receiver line. Inside a cross-spread, all spatial attributes vary smoothly. However, cross-spreads have limited extent, because offset increases towards the edges of the cross-spread, such that at some point a maximum useful offset is reached. The edges of the cross-spreads constitute unavoidable spatial discontinuities. Spatial continuity can be maximised by utilising the maximum useful offset in both horizontal (in-line and cross-line) directions, thus creating the largest possible cross-spreads with useful extent. Essentially, this leads to a wide geometry in contrast to a narrow

geometry where the maximum cross-line offset is considerably smaller than the maximum in-line offset.

Conventional processing of 3D data is basically an extension of 2D processing. For parallel acquisition geometry (parallel source lines parallel to parallel receiver lines), which looks like repeated acquisition of 2D lines, this approach is satisfactory. However, an orthogonal geometry has entirely different properties and needs a different approach to prestack processing. As a first step in that direction, Vermeer (1994, 1998a) proposed the use of cross-spread-oriented prestack processing to exploit the spatial continuity in the cross-spread acquired with symmetric sampling.

Cross-spreads belong to a class of single-fold data sets called minimal data sets (MDSs) (Padhi and Holley, 1997). An MDS is suitable for imaging that part of the subsurface volume, which it has illuminated. Because of the limited extent of the cross-spread, only a limited part of the subsurface can be imaged, and the images are incomplete around the edges of the cross-spread. What one would really like to have are MDSs, which extend across the whole survey area. As such MDSs do not exist in an orthogonal geometry, one could try to construct *pseudo*-minimal data sets (pMDSs), which extend across the whole survey area, and deviate as little as possible from a true MDS. The construction of pMDSs was discussed in Vermeer (1998c). In that paper, the pMDSs were applied for the creation of common image gathers (CIGs).

In the present paper, I am introducing a much wider assortment of pMDSs, which can be constructed from regularly sampled orthogonal geometries. It turns out that each prestack processing step can benefit from a reasoned selection of pMDS on which to operate; one process benefiting from quite a different choice than another.

This paper consists of the following main parts. First, a summary is given of 3D symmetric sampling and the properties of the orthogonal geometry and its basic subset, the cross-spread. Then the assortment of pMDSs is introduced and explained. For a number of prestack processing steps the selection of the most suitable pMDSs is discussed.

## ***3D symmetric sampling of orthogonal geometry***

### **3D subsets of 5D prestack wavefield**

In 2D the sampling problem is one of sampling the 3D wavefield  $W(t, x_s, x_r)$  with temporal coordinate  $t$ , source coordinate  $x_s$ , and receiver coordinate  $x_r$ . In 2D symmetric sampling the two spatial (source and receiver)

coordinates are sampled in the same way. Using sufficiently small sampling intervals allows the faithful reconstruction of the underlying continuous wavefield, i.e., it maintains the spatial continuity of the wavefield  $W(t, x_s, x_r)$ .

In 3D we are faced with the sampling of a 5D wavefield  $W(t, x_s, y_s, x_r, y_r)$ , now with source  $y_s$  and receiver  $y_r$  as additional spatial coordinates. It would be prohibitively expensive to completely sample this 5D wavefield, as this would mean filling the whole survey area with a dense coverage of both sources and receivers. As a compromise, 3D symmetric sampling settles for the more affordable aim of correct sampling of overlapping single-fold 3D subsets of the 5D wavefield  $W(t, x_s, y_s, x_r, y_r)$ .

Each common acquisition geometry has its typifying basic subset. Table 1 lists some of them. In a common-offset vector (COV)-gather, the offset vector  $(X, Y)$  is the same for each trace (in-line offset  $X$ , cross-line offset  $Y$ ); it is also called common-offset gather with constant azimuth.

**TABLE 1 EXAMPLES OF BASIC SUBSETS**

Basic subset	Source coordinates	Receiver coordinates	Acquisition geometry
Midpoint line	$(x_s, Y_1)$	$(x_r, Y_2)$	Parallel
COV gather	$(x_s, y_s)$	$(x_s + X, y_s + Y)$	Parallel
Cross-spread	$(X, y_s)$	$(x_r, Y)$	Orthogonal
Slanted spread	$(X + x_s, Y + \alpha x_s)$	$(x_r, Y)$	Slanted
Zig spread	$(X + x_s, Y + x_s)$	$(x_r, Y)$	Zigzag
3D shot	$(X, Y)$	$(x_r, y_r)$	Areal
3D receiver	$(x_s, y_s)$	$(X, Y)$	Areal

$X$  and  $Y$  are fixed, lower case coordinates vary.

Considering each source line and each receiver line in the line geometries as a continuous coverage of sources and receivers along those lines leads naturally to the basic subsets of the line geometries (geometries in which sources and receivers are located along individual lines rather than in areas). A basic subset is formed by all traces that have a source line and a receiver line in common. For orthogonal geometry, the basic subset is called the cross-spread. In slanted geometry we have slanted spreads, and in parallel geometry the combination of a source line and a receiver line is just the midpoint line. In the ideal parallel geometry, the COV gather is another 3D subset.

All basic subsets are also single-fold, except the midpoint line. The midpoint line does not provide areal coverage, whereas the other subsets do.

The number of overlapping single-fold subsets at any point determines the fold-of-coverage in that point. These subsets are also called MDSs because they constitute the lowest-fold data sets, which are suitable for prestack migration.

This paper is concentrating on the orthogonal geometry, which is most commonly used in land data acquisition and in OBC acquisition. Its basic subset, the cross-spread, is discussed in more detail in the next section.

### **Cross-spread as subset of orthogonal geometry**

In the field, the data of an orthogonal geometry are acquired in swaths or templates, which may consist of a series of shots (sometimes called a shot salvo) shooting centre-spread into the active receivers of an even number of receiver lines (see left part of Figure 1<sup>1</sup>).

Cross-spreads can be extracted from the orthogonal geometry by collecting all traces that have a source line and a receiver line in common. Hence, there are as many cross-spreads as there are intersections between source lines and receiver lines. The right part of Figure 1 highlights the shots and receivers corresponding to one cross-spread in the same orthogonal 3D survey, as shown on the left.

Figure 2 illustrates some of the properties of the cross-spread. The trace at midpoint  $M$  is a member of a common-shot gather, a common-receiver gather, a common-offset gather, and a common-azimuth gather. Each trace in the 3D survey is an element of a unique cross-spread. The neighbours of the trace in the cross-spread have been shot by the same shots or by adjacent ones, and have been recorded by the same receivers or by adjacent ones. Hence, the spatial attributes of the traces around  $M$  vary slowly, making the cross-spread a spatially continuous data set. On the other hand, the edges of the cross-spreads form spatial discontinuities.

After the swath has rolled sideways across the whole width of the survey area, it is always rolled in the cross-line direction over a distance equal to the shot salvo. This ensures a constant cross-line fold-of-coverage. The template shown in Figure 1 corresponds to the "single-line roll". This single-line roll ensures that all cross-spreads are acquired with maximum cross-line offsets that are the same on both sides of the receiver spread (symmetric cross-spreads). Swath implementations with shot salvos equal to a higher multiple of the receiver line interval are also in use. For these multi-line roll geometries,

---

<sup>1</sup> Figures are located at end of this text.

the acquired cross-spreads are asymmetric. Multi-line roll acquisition is more efficient than single-line roll, but it will lead to irregularities in the bin attributes across the survey, and it will hamper the creation of pMDSs for the whole geometry.

### **3D symmetric sampling**

Symmetric sampling was introduced for 2D lines in Vermeer (1990), whereas the concept was extended to 3D in Vermeer (1994). In the 3D symmetric sampling approach, we attempt to properly sample the single-fold subsets of the chosen geometry. This is achieved by dense enough sampling of the varying coordinates in each subset (cf. Table 1). Usually, sampling of a subset will provide a single-fold (except in the case of sampling the 2D line) data set of limited extent. As can be understood by inspection of Figure 1 for an orthogonal geometry, partially overlapping subsets need to be sampled to cover the whole survey area.

Often the extent of the basic subsets is maximised in only one spatial direction. A large extent in both spatial directions would fully exploit the potential of each geometry. Therefore, besides alias-free sampling of the basic subsets, we should maximise the (useful) areal extent of the subsets with limited extent. This prescription maximises the spatial continuity in the 3D survey and, for a given fold, minimises the number of edges in the survey.

Besides the 2D symmetric sampling requirements of equal shot and receiver intervals and equal shot and receiver arrays, 3D symmetric sampling of orthogonal geometry also requires as many receivers in the common shot as shots in the common receiver, and the centre-spread acquisition of both shots and receivers. This recipe ensures the acquisition of square cross-spreads (the aspect ratio of the geometry equals one, as in the example of Figure 1). The source line interval and the receiver line interval should preferably be the same for symmetric sampling as well.

## ***Selection of pseudo-minimal data sets***

### **Building fold with basic subsets**

The cross-spread is a MDS with limited extent. For quite a few processing steps, it would be helpful to avail of MDSs which extend across the whole survey area. As these do not exist in an orthogonal geometry, we have to look for pMDSs which can be constructed from the available data and which are as close as possible to an MDS.

In this chapter it is shown that a plethora of pMDSs may be constructed from regularly sampled acquisition geometry. For a better understanding of the various forms of pMDSs, it is helpful to describe first how fold-of-coverage is built in an orthogonal geometry.

Consider the cross-spread in Figure 1. The width of the midpoint coverage in the in-line (receiver line) direction  $W_x$  is

$$W_x = (\text{receiver spread length}) / 2 \quad (1)$$

The in-line fold  $M_x$  equals the number of times the source line interval  $SLI$  fits on the width of the in-line coverage

$$M_x = W_x / SLI \quad (2)$$

Similarly, the width of the midpoint coverage in the cross-line (source line) direction  $W_y$  is

$$W_y = (\text{shot spread length}) / 2, \quad (3)$$

where shot spread is the part of the source line being listened to by the receivers in the receiver spread. The cross-line fold  $M_y$  equals the number of times the receiver line interval  $RLI$  fits on the width of the cross-line coverage

$$M_y = W_y / RLI \quad (4)$$

Total fold-of-coverage  $M$  is

$$M = M_x M_y \quad (5)$$

The total fold equals the number of overlapping midpoint areas (the grey areas in Figure 1) in any point. This is further illustrated in Figure 3, where overlapping cross-spreads are shown for a geometry with  $M_x = 4$  and  $M_y = 2$ .

If  $M_x$  or  $M_y$  are not integer, then the number of traces in the CMPs of the geometry is not the same everywhere. Therefore, for regular fold, it is necessary that  $W_x = n SLI$  and  $W_y = n RLI$ .

In Figure 3, coverage is shown for a single unit cell (the dark area in the lower part of the figure). The size of the unit cell equals the area between two adjacent receiver lines and two adjacent source lines. Figure 3 illustrates that for fold  $M$ , the area of the cross-spread can be subdivided into  $M$  areas with the size of a unit cell.

In 3D, offset can be described by  $x$ - and  $y$ -components, the in-line offset and the cross-line offset. Half offset as  $\mathbf{h} = (h_x, h_y)$ . Therefore, an appropriate name for the unit-cell-sized subareas in the cross-spread is offset-vector slot (OVS). Each OVS is built from a limited range of shots along the source line

and a limited range of receivers along the receiver line (Figure 4). These two ranges restrict the range of offset vectors to a small slot. Figure 5 illustrates the variation of offset and azimuth of the centre of each OVS in a cross-spread. OVSs are important building blocks for pMDSs.

An OVS can be characterised by four parameters,  $OVS = OVS(h_x, h_y, \Delta h_x, \Delta h_y)$ , where  $h_x$  and  $h_y$  are the half-offset coordinates of the centre of gravity of the OVS, and  $\Delta h_x$  and  $\Delta h_y$  describe the range of half-offsets in  $x$ - and  $y$ -direction. (In a cross-spread centred coordinate system,  $h_x$  and  $h_y$  equal the midpoint coordinates:  $x_m = h_x$ ,  $y_m = h_y$ .) In a cross-spread which is symmetric with respect to both axes (centre-spread acquisition for both receiver spread and source spread), each OVS has counterparts in the other three quadrants with the same absolute values of its four parameters. Of these four OVSs, the pairs in opposite quadrants have also opposite, i.e., similar shot/receiver azimuths (cf. Figure 5).

### **Fold, illumination and imaging**

Some general definitions before starting with pMDS construction.

For each MDS we can define a midpoint area (the area covered by the midpoints), an illumination area (the area on the reflector illuminated by all shot-receiver pairs), and an image area (the area on the reflector for which correct imaging is possible). Should a number of MDSs have overlapping midpoint areas, then we may define

"fold-of-coverage": number of overlapping midpoint areas,

"illumination fold": number of overlapping illumination areas, and

"image fold": number of overlapping image areas.

In general, illumination fold will not be very different from fold-of-coverage, though it may be locally higher or lower. Image fold is the same as illumination fold, if we neglect edge effects. Fold-of-coverage and image fold provide a statistical means of suppressing noise. If the data are properly sampled, fold is not necessary to improve the migration result itself, because single-fold data are sufficient for imaging.

### **Construction of pMDSs**

Even though cross-spreads have limited extent, it is possible to create single-fold coverage across the whole survey area by a tiling of adjacent cross-spreads. In such a single-fold gather, the data is piecewise continuous, with discontinuities between the adjacent cross-spreads (see Figure 6). Figure 7

shows the illumination by four adjacent cross-spreads of a reflector with 15° dip and a reflector with 45° dip. Each cross-spread covers the reflector with its own “blanket.” Around the edges of these blankets gaps and overlaps exist. Within each blanket, illumination can be considered as continuous (provided the cross-spread is sampled alias free), but illumination is discontinuous across the edge of each blanket.

A tiling of adjacent cross-spreads as in Figure 6 is the first example of a pMDS (Vermeer, 1998c). The number of different tilings equals the fold-of-coverage. It is clear from Figure 7 that these tilings cannot produce good images of the subsurface everywhere. Locally, the images will show considerable artefacts, depending on the dip of the reflectors being imaged. Therefore, it would be desirable to find a single-fold coverage using data with smaller discontinuities. As the discontinuities of the cross-spreads are a given, the only way to reduce their effect is by spreading the discontinuities thinly over the survey area. This can be done by selecting tilings of OVSs as illustrated in Figure 8. In such a tiling or OVS gather, the frequency of spatial discontinuities is much higher than in adjacent cross-spread tilings. Their magnitude, however, is much smaller.

Cary (1999) also introduced the OVS gather as a basic building block of wide-azimuth surveys. He called them common-offset vector (COV) gathers, which would be a bit too optimistic as offset still does vary across each tile of the gather. Yet, I like the expression "offset vector", and therefore, I introduced here the expression offset vector slot, which was called offset/azimuth slot in Vermeer (1998c). COV gather is a more appropriate name for the subset of the ideal parallel geometry.

### **A measure of spatial discontinuity**

Let us consider a subdivision of a cross-spread into OVSs as in Figure 5. Then the horizontal width of the OVS  $\Delta h_x$  [cf. equation (2)]

$$\Delta h_x = W_x / M_x = SLI, \quad (6)$$

and the vertical width  $\Delta h_y$

$$\Delta h_y = W_y / M_y = RLI \quad (7)$$

The offset discontinuity across the vertical edges of an OVS equals  $\Delta h_x$ . This discontinuity occurs along a length  $\Delta h_y$ . So, a representative measure of the total discontinuity across the length of a vertical edge of an OVS might be  $\Delta h_x \Delta h_y$ . The same expression is found for the discontinuity across each

horizontal edge, for a total discontinuity of  $4 \Delta h_x \Delta h_y$ . The OVS shares this discontinuity with four other OVSs, so the average discontinuity per OVS  $D_{OVS}$  may be characterised by

$$D_{OVS} = \Delta h_x \Delta h_y = SLI \cdot RLI, \quad (8)$$

which is the area of the OVS. Hence, the spatial discontinuity in an OVS gather per unit area equals 1.

In a tiling of adjacent cross-spreads, the spatial discontinuity across a cross-spread  $D_X$  could be derived in a similar way as for an OVS, leading to

$$D_X = W_x W_y, \quad (9)$$

which equals the area of the cross-spread. Therefore, the spatial discontinuity in a tiling of adjacent cross-spreads also equals 1.

My definition of spatial discontinuity implies that the amount of spatial discontinuity for a given geometry is invariable, but that its local density can be varied. The smaller the unit cell of a geometry, the smaller the discontinuities inside OVS gathers can be.

It should be noted that the measure of spatial discontinuity introduced here is not sufficient to predict the effect of the discontinuity. The effect also depends on the average absolute offset of the OVS gather; the larger that offset, the stronger the effect in general. It also depends on the dip of the events, the larger the dip the larger the discontinuities.

### **A plethora of OVS gathers**

Up till now, the cross-spread has been subdivided into OVSs, which taken together fill the whole cross-spread. However, a single-fold OVS gather can also be constructed using a generating OVS  $(h_x, h_y, \Delta h_x, \Delta h_y)$ , which still has the size of a unit cell, but which can be located anywhere inside the cross-spread, i.e., OVS  $(h_x, h_y, SLI, RLI)$ , with  $|h_x| < (W_x - SLI)/2$  and  $|h_y| < (W_y - RLI)/2$ . This will increase the flexibility of selecting suitable OVS gathers considerably.

A generating OVS may also consist of  $n \times m$  unit-cell sized areas together. Taking the same area of each cross-spread in this way leads to  $n \times m$  fold OVS gathers. Higher fold in an OVS gather may be useful for high-fold data, or for noisy data.

For any single-fold tiling of the survey area it is necessary that the tiles have dimensions  $SLI \times RLI$  or multiples thereof. However, in some cases it may be desirable to construct the tiles from smaller OVSs. For instance, along

the  $x$ -axis, OVS  $(\pm h_x, 0, SLI/2, RLI)$  may be used (Figure 9). This implies the use of an OVS with the area of half a unit cell and its mirror image. Similarly, along the  $y$ -axis we have OVS  $(0, \pm h_y, SLI, RLI/2)$ . It is of interest to investigate the spatial discontinuity of these OVSs.

In the juxtaposed bottom corners of the OVS along the  $x$ -axis, the offset vectors are  $(H_x + SLI/2, -RLI/2)$  and  $(-H_x - SLI/2, -RLI/2)$ . Using reciprocity, the second offset vector may also be written as  $(H_x + SLI/2, RLI/2)$ . Hence, the discontinuity in offset vector at that point equals  $-RLI$ . Along the  $x$ -axis the juxtaposed offset vectors are  $(H_x + SLI/2, 0)$  and  $(-H_x - SLI/2, 0)$ . With reciprocity these two are the same, i.e., there is no discontinuity along the  $x$ -axis. Using the same reasoning for the juxtaposed top corners of the OVS, there the discontinuity equals  $RLI$ . Hence, the discontinuity along the vertical varies between 0 and  $RLI$  along a distance  $RLI$ . So, the measure of spatial discontinuity across the vertical equals  $RLI RLI / 2$ .

Across the horizontal boundaries, the same OVSs are found, with a constant jump of  $RLI$  in the  $y$ -coordinate and no discontinuity in the  $x$ -coordinate. Hence, along the horizontal the measure of spatial discontinuity equals  $RLI SLI / 2$ . For  $SLI = RLI$ , the spatial discontinuity associated with each OVS again equals its size, i.e.,  $D_{OVS} = RLI SLI / 2$ . If  $RLI < SLI$ , the spatial discontinuity of OVSs along the  $x$ -axis is smaller than the OVS size, whereas for OVSs along the  $y$ -axis it would be larger than the OVS size, and vice versa for  $RLI > SLI$ .

Finally, for situations where azimuth does not play a role, unit cell sized tiles may be constructed from four small OVSs (Figure 9). This collection can be described by OVS  $(\pm h_x, \pm h_y, SLI/2, RLI/2)$ .

## ***Application to prestack processing***

### **Introduction**

In the following sections, ideas are put forward for the most suitable input gathers for noise removal, muting, first-break picking, residual statics picking, velocity analysis, AvO and AvAzimuth, velocity model updating, and prestack migration.

As different tasks need different data gathers, either much sorting has to be done to feed the different gathers to the various processing steps or random access should be available. Sorting is very time-consuming, whereas random access is fast, but it requires a database with pointers to the correct trace positions. Eventually, random access is going to take over (Jack, 1999).

## Noise removal

The ground roll energy tends to be partially aliased, because of its slow velocity. The non-aliased part of the ground roll (and even a bit more) can be removed by prestack velocity filtering. The obvious input gather for this process is the cross-spread, so that noise can be removed either by cascaded application of shot and receiver domain  $fk$  filtering, or by a 3D velocity filter.

In an OVS gather with  $SLI \times RLI$  sized slots (or smaller) the spatial discontinuities of the non-aliased part of the ground roll tend to be even larger than across cross-spread boundaries. Across cross-spread boundaries there is usually no ground roll, except perhaps at larger times. Each OVS that cuts through the ground roll shows discontinuities in the noise at its edges. Therefore, it is important to remove the ground roll as much as possible prior to any spatial processes applied to OVS gathers. A particularly powerful technique, which also removes much of the aliased ground roll, was discussed in Miao and Cheadle (1998).

## Muting

At first sight, it might seem strange to require a specific input sorting for an optimal mute application. Indeed, the idea here is not to use a different sorting, but to learn from the insights gained in the previous chapter about the many different OVSs into which a cross-spread may be subdivided.

The unit cell of a regular orthogonal geometry represents the 2D periodicity of the acquisition geometry. Usually, the acquisition imprint shows this same periodicity. The visibility of the acquisition imprint may be caused by two main factors: (1) variability of effective fold inside the unit cell for times where traces with larger offsets are muted, and (2) the unit cell periodicity in the offset distribution. There is little one can do about the periodicity, but the variability of fold can be easily removed.

Consider Figure 9. Taking eight quarter-unit-cell sized OVSs as indicated with the chequered squares and the striped squares, then each of those OVSs has the same absolute offset distribution. The same mute time can be assigned to all traces inside these squares. If this procedure is carried out for all OVSs with the same absolute offset distribution, the effective fold-of-coverage will be constant for constant time. This should reduce the acquisition imprint of the geometry. It would be interesting to check this using real data acquired with a regular orthogonal acquisition geometry.

Hill et al. (1999) show a clear correlation between time slice amplitude and the fold of data contributing to the time slice. They used synthetic data

acquired with zigzag geometry. The muting proposed here for the orthogonal geometry could also be adapted to other regular acquisition geometries. If applied to their data, the acquisition footprint would be removed almost entirely.

### **First-break picking**

In first break picking, only the near-surface variation plays a role. The time picks depend on offset and location. Per definition, the traveltimes differences due to differences in offset are zero in a common-offset gather. Therefore, picking in common-offset gathers has to overcome the smallest time differences; hence, this would be easiest and most successful.

The nearest to a common-offset gather one has in an orthogonal geometry is the OVS gather of which an example is shown in Figure 8. Therefore, picking in OVS gathers might be a good starting point. All  $M$  OVS gathers are potential candidates for picking, but some of them may drop out due to quality problems.

In case there are serious picking problems, it may be beneficial to combine OVS gathers for mirror OVSs in the opposite quadrant, as these have about the same azimuths. It may be more difficult to combine mirror OVSs in adjacent quadrants, as these have different azimuths and may have different traveltimes.

An alternative to picking in gathers of ( $SLI$ ,  $RLI$ )-sized OVSs is picking on a per cross-spread basis. The advantage of this alternative is that the area with spatial continuity in a cross-spread is much larger than in an OVS gather. The disadvantage is that the large spatial discontinuity between cross-spreads might necessitate to start picking afresh for each cross-spread.

The more flexible approach is to combine picking in the OVS gathers with picking in the cross-spreads. Especially in combination with the nearest-neighbour approach to picking (see next section), this should give the best results.

### **Nearest-neighbour correlations**

Conventional first-break picking and reflection time picking techniques are based on a sequential approach (Cox, 1999). Often, picking and statics computation are mixed into one operation. Here I propose to carry out the picking in an areal approach, using nearest neighbours, and also to separate the two actions: first carry out all picking and verify the results, and then feed the verified picks to the statics computation procedure (Vermeer, 1990, Ch. 5.7).

In the nearest-neighbour approach, each trace is cross-correlated with its eight nearest neighbours. This has the advantage of comparing traces with a minimum of difference in character between them. Another advantage is that it leads to redundant picking, which allows correction of mispicks before these are used in the statics computation procedure. Redundancy exists for every closed loop between traces: the sum of the corresponding time shifts should equal zero. Once all mispicks have been solved, all time shifts can be integrated into a single time surface across the area of the picked times.

This procedure was proposed in Vermeer (1990, Ch. 5.7) for 2D data, but it applies just as well or even better to 3D data. All mispicks might first be solved for a number of single-fold OVS gathers, and by making links between the gathers (via cross-spread continuity), the picks might even be made consistent in a 3D sense ( $x$ ,  $y$ , and fold).

It should be realised that the spatially nearest neighbours in an OVS gather are not always nearest neighbours in 5D space, because of the spatial discontinuity which still exists across the edges of neighbouring OVSs. Again, the picking redundancy should help to solve any problems in linking time shifts across these boundaries.

### **Residual statics**

Picking of time shifts for residual statics analysis in 3D data usually takes place in bins or in a small group of bins. Each trace in a bin corresponds to a different cross-spread; therefore, consecutive traces sorted according to absolute offset, may have entirely different azimuth and originate from widely spaced cross-spreads. This is illustrated in Figure 10, where trace positions are displayed according to their  $(h_x, h_y)$  coordinates inside each bin. Traces with mirrored positions inside these bins have about the same absolute offset.

Determining time shifts between traces using nearest neighbours (as proposed in the previous section), ensures that the difference in character between traces that are to be compared is as little as possible. Moreover, it allows removal of mispicks even before the statics computation procedure is entered.

The time differences established in nearest neighbour communities are not only composed of static differences, but also of structure and velocity differences. Moreover, there is picking noise. To compute the statics from the time shift surfaces across the survey area, new algorithms are required. These algorithms should make use of the special properties of static differences, which are very different from differences due to structure variations or velocity

variations. Note that velocity determination prior to residual statics determination is no longer necessary. A very rough NMO correction may be applied, or no NMO at all, prior to the time shift measurements. This is an advantage, especially for wide orthogonal geometries, because velocity determination is best carried out after DMO, whereas statics should be determined prior to DMO.

## **Velocity analysis and DMO**

Conventional velocity determination after DMO splits the input data into small offset ranges, each offset range is DMO'ed separately, followed by gathering of the results per bin and semblance analysis. In a parallel geometry or in a narrow orthogonal geometry, this procedure should work satisfactorily. However, in a wide geometry, common offset-range gathers have a very irregular fold, and are not likely to produce well-resolved DMO images. A common offset-range gather is shown in Figure 11. It illustrates the irregular fold, and shows the many edges in such a gather.

Several authors showed that cross-spreads are suitable for DMO (Vermeer et al., 1995; Collins, 1997; Padhi and Holley, 1997). It should be possible to obtain good quality DMO images for the interior part of each cross-spread. However, offset varies inside a cross-spread and as a consequence, each image is made up of different offsets and the offset attached to each DMO image is not known anymore. To determine velocity, it is still necessary to split the data over offset ranges.

The smallest offset ranges, which still give complete single-fold coverage, can be found along the acquisition lines as indicated in Figure 9 with the grey rectangles. For an in-line fold of 6, there are 6 different OVS gathers with disjoint offset ranges. If the geometry would also be 6-fold in the cross-line direction, another 5 OVS gathers can be made from OVSs along the source line. For a maximum in-line offset and a maximum cross-line offset of 3000 m, the range of offsets in any OVS gather would still be at least 500 m. Hence, the uncertainty about the offset at the image point is still quite large.

In a low-relief geology, the DMO shift is small, and it would be sufficient to select points in the centre of the tiles of each OVS gather as locations for velocity determination. The offsets in these points can be used to estimate the velocity in those points.

In a steeper dip situation, the (unknown) offset of the image trace and the offset of the input location will differ considerably, and this would lead to systematic errors in the velocity estimates. In these situations, it may be better

to try a velocity scanning procedure (i.e., apply DMO after many different NMO corrections) rather than a semblance measurement. Usually, the velocity determination is restricted to some discrete points across the survey area. Using only a restricted subset of the input data - the offset vector slots around the acquisition lines - a scanning procedure would still be cost-effective.

Of course, there are many variations possible on this theme. The main point is to select good input data gathers to ensure the best possible images with the least amount of edge effects.

Should the total fold along the two orthogonal directions not be sufficient for accurate measurements, OVS gathers using different OVSs may be used, in particular those in the far corners of the cross-spread having the largest absolute offsets. The measurement of velocity in OVS gathers taken along two orthogonal directions, also allows recognition of velocity anisotropy under suitable circumstances.

## **AvO**

The determination of AvO parameters from an orthogonal geometry is one of the most challenging tasks. The main problem is that proper common offset gathers are not available for analysis; moreover the trace density per offset increases with increasing offset. It is also difficult to give a general recipe for AvO analysis, because there are so many different types of problems. In some cases, one would like to scan a large time window for possible AvO anomalies; in other cases specific horizons are to be investigated, and then these horizons may or may not need prestack migration. Whatever the AvO problem is, I expect that solutions will have to be sought in a judicious use of OVS gathers. In this section, I am restricting myself to giving some suggestions to be tried for a horizon-specific AvO problem.

Of course, the advantage of a horizon-specific problem is that processing can be target oriented, so that not all data have to be processed, albeit that all traces have to contribute. The basic input for the analyses would be OVS gathers of unit-cell sized disjoint OVSs, i.e.,  $M$  OVS gathers as indicated in Figure 5. Depending on the problem, these gathers would be either NMO-DMO'ed or prestack migrated, followed by stacking.

The next step would be to pick the horizon on the stacked data volume, followed by making horizon slices according to these picked times in the contributing OVS gathers. The OVS gathers can be stacked pairwise with their mirror OVS gather in the opposite quadrant. (This should not be misinterpreted as stacking of data from opposite parts of the same cross-spread; the data to be

stacked has the same midpoint coordinates and originates from different cross-spreads.) Accepting that the spatial resolution of the AvO analysis will be restricted to approximately the size of a unit cell, the horizon amplitudes can now be analysed in  $M/2$  overlapping unit-cell sized slots as indicated in Figure 12.

If the amplitudes are averaged in a ring-shaped area corresponding to some range of offsets, the pairwise stacking may be just as well omitted from this procedure. For odd  $M$  not all OVSs can be paired.

The procedure described here will break down if the migration distance becomes significant. Then there will no longer be a direct relationship between position inside a slot and the offset of the migrated image. A solution of this problem is discussed in the chapter on prestack migration. Tura et al. (1998) show the importance of prestack migration for AvO analysis for data acquired with parallel geometry.

If the slots are small, offset does not vary much across each slot and the average amplitude in the slot may be considered representative for the average offset of the slot. In low-relief situations, another acceptable way of reducing the size of the slots, is to use  $M$  disjoint ( $SLI/2$ ,  $RLI/2$ ) sized slots as indicated by the chequered slots in Figure 9.

### **Amplitude versus azimuth**

For analysis of azimuth-dependent effects, the same procedure can be applied as proposed for AvO in the previous section. Again, unit-cell sized areas of the survey have to be taken together, but split over the  $M$  different OVSs. Pie slices taken from the collection of data represent data with the same azimuth range (Figure 12). Now amplitude behaviour has to be analysed on a per pie slice basis. Note that the arrows indicating the average azimuth in each slot do not have the same direction as the orientation of the pie slice.

### **Velocity-model updating**

The process of velocity-model updating can be subdivided into two major steps: (1) the creation of images using subsets of the total data set, followed by (2) an analysis procedure to find an improved velocity model. The collection of all image traces for a given point is called common-image gather (CIG). The first step in the analysis procedure is to measure the imaged time or depth for a particular reflection; for a correct velocity model, this time or depth is the same for all images in a CIG.

For a successful velocity model-updating procedure, it is essential that the images produced in step 1 are clean and do not suffer from artefacts. In parallel geometry, the obvious subset for creating CIGs is the common-offset gather. Firstly, it should produce clean images (usually a small range of offsets has to be taken as input to ensure complete coverage), and secondly, errors in velocity can be directly related to offset. As discussed before and shown in Figure 11, proper common-offset gathers cannot be extracted from an orthogonal geometry. This will pose considerable extra challenges for the velocity-model updating procedure to be used for this geometry.

It is tempting to use complete cross-spreads for imaging as each cross-spread is capable of producing clean images for a large part of the volume which it has illuminated. However, the area where clean images occur for a cross-spread is unpredictable without further analysis (it might be predicted using the current velocity model), and that area would be different for different overlapping cross-spreads. Using a tiling of adjacent cross-spreads as in Figure 6 would produce clean images in some places and strong artefacts in other places. A better alternative might be to use OVS gathers as described in Figure 8.

Whether cross-spreads or OVS gathers are used for imaging, the problem remains that the offset of the imaging trace is not known without further action. This is caused by the variation in offset that occurs across a cross-spread and still occurs across the OVS gather. Earlier I proposed to use the vector-weighted diffraction stack (Vermeer, 1998) to determine the offset corresponding to each image. Tura et al. (1998) applied that technique for AvO analysis. They did not use it to determine the offset in the image (they were using common-offset gathers as input, hence knew the offset already), but to determine reflection coefficient and reflection angle. The recipe of the vector-weighted diffraction stack is given in Tygel et al. (1993) who expanded an earlier idea proposed in Bleistein (1987). Unfortunately, the vector-weighted diffraction stack is quite sensitive to noise, because it depends on measurements made on the basic input data.

A better way to find the offset in the image point is a modification of an idea proposed in Harris et al. (1998). In their MITAS procedure they consider the volume of data being used to build a single image trace. The procedure consists of the following steps:

1. Flatten the diffraction traveltime curves in the input volume; this will lead to bowl-shaped events for the reflections;

2. Stack the new volume in two orthogonal directions; this will improve the signal-to-noise ratio of the data to be analysed;

3. Determine the points of stationary phase of the major reflections in both stacks; the two points for each reflection will determine the position in the input volume of the image point.

Harris et al. (1998) use this procedure to determine an area around the image point that will be included in the imaging process, whereas the data outside this area will be discarded. In this way migration aliasing noise is avoided and a cleaner image can be produced, in particular for coarsely sampled data. However, knowing the position of the image trace also means that its offset can be retrieved and be used for further analysis in the velocity-model updating procedure.

Using OVS gathers for this analysis provides the best chances for clean images and also allows the determination of the offset in the image point. Yet, the irregularities associated with the spatial discontinuities in the OVS gathers may still hamper an accurate analysis, especially if the image point is close to the edge of an OVS. To compensate for that situation, it may be considered to carry out the analysis as well for OVS gathers based on OVSs shifted over ( $SLI/2$ ,  $RLI/2$ ). Again, to minimise the amount of work to be carried out for this analysis, it should be considered to restrict the analysis to discrete locations and to specific target horizons.

### **True amplitude prestack migration of regular and irregular data**

In this section, a synthesis is made of ideas described by Harris et al. (1998, see previous section), Albertin et al. (1999), Bloor et al. (1999), and Rousseau et al. (2000), supplemented with some further ideas.

Albertin et al. (1999) describe that for most acquisition geometries, even if acquired in a rather regular way, it is difficult to give an analytic expression of the Beylkin determinant (Bleistein, 1987), needed in true amplitude migration. Instead, they came up with the idea of measuring the dip angles being illuminated in the output point by all the shot/receiver pairs in a data set. The dip angle illuminated by a single shot/receiver pair and its corresponding wavenumber vector is illustrated in Figure 13. All shot/receiver pairs together determine the range of dips that can be illuminated by the data set. Albertin et al. (1999) propose to equalise the distribution of angles across the unit sphere in the output point by weighting according to the local density of wavenumber vectors on the unit sphere. They show that this is equivalent to applying

Beylkin's determinant. The technique not only corrects for irregular geometry but also for refraction effects in the overburden.

Bloor et al. (1999) apply Albertin's method to data acquired with a spider-web geometry (this is a geometry with radial receiver lines and circular source lines). They show that this technique leads to considerable improvement of data quality. In this application no distinction is made between data with different offsets or coming from different subsets: each shot/receiver pair in the total data set contributes its own angle and its own point on the unit sphere. Figure 2 in Bloor et al. (1999) shows the midpoints for all traces with a small offset range. It leads to a similar figure (interlocking rings) as shown in Figure 11. This means that the spider-web geometry, even though apparently quite irregular, does have some regularity attached to it as well.

Rousseau et al. (2000) carry Albertin's idea a bit further and suggest to apply it to the MDSs of the acquisition geometry. They illustrate this with common-offset data retrieved from a parallel geometry. Applying the technique to subsets of the data makes it suitable for better AvO analysis, and it does not mix up effects from widely different shot/receiver pairs. On the other hand, the low fold of an MDS may easily lead to gaps in the range of dips being illuminated. Weighting of the traces around such gaps has two effects: (1) if the gap occurs in the flat part of the bowl-shaped reflection events (after application of diffraction traveltimes surface flattening, see previous section), then weighting will ensure a better amplitude of the image, but (2) if the gap occurs in the steep part of the bowl-shaped reflections, weighting of the traces will increase aliasing artefacts. This is clear from Figure 3 in Rousseau et al. (2000), where not only reflection amplitude is improved by weighting but an artefact caused by some missing in-lines is enhanced as well.

The ultimate synthesis of all ideas is to use OVS gathers (pairwise, as discussed for AvO analysis), to establish the point of stationary phase using Harris et al.'s (1998) method, and applying aperture limitation around that point, followed by Albertin weighting in the remaining area (where aliasing does not occur).

## **Illumination and imaging with OVS gathers**

In this section a first and very modest step is set towards testing the ideas discussed in the previous sections. The test model consists of a reflector with 15° dip in a medium with constant velocity of 3000 m/s. The depth of the reflector is 3000 m in the centre of the model. Source and receiver line spacings of the 36-fold orthogonal geometry are 400 m, and the station intervals are 50 m. Figure 14 shows illumination by various OVS gathers.

Except for Figure 14f, the reflector dips always in an easterly direction. Figure 14a used the OVS from the upper right corner of each cross-spread with average  $\mathbf{h} = (1000, 1000)$ . In this case the spatial discontinuity between the OVSs translates in vertical illumination gaps and horizontal overlaps. The reverse is the case with the OVS from the opposite side of the cross-spread shown in Figure 14b. The illumination by these two OVS gathers is the most discontinuous of all possible gathers. It is interesting to see that their combination leads to an almost regular 2-fold illumination as shown in Figure 14c.

Figure 14d shows that illumination by complete cross-spreads is more continuous overall. However, the overlaps and the gaps are larger than in the case of the OVS gathers. Figure 14e and f show illumination by pairs of rectangles at the far end of the receiver line (average  $|\mathbf{h}| = (1100, 0)$ ). In Figure 14f the reflector makes an angle of  $45^\circ$  with the receiver line. In Figure 14e two-fold and zero-fold illumination alternate in thin horizontal strips, whereas everywhere else illumination is single-fold. In Figure 14f the irregularities are spread even more thinly.

Figure 15 shows migration results corresponding to Figure 14. Each figure shows a horizon slice through a migration result. Not unexpectedly, the images show a clear correspondence to the illumination areas. It is interesting to note, that the amplitude variation in Figures 15e and f is smaller than in Figures 15a and b, which suggests that OVS gathers composed from OVSs along the acquisition lines are most suitable for application in velocity-model updating.

All figures show weakening of amplitudes towards the left. This is caused by not compensating for the smaller Fresnel zones at shallower depths. The very weak amplitudes in the centre of Figure 15d reflect the illumination gap shown in Figure 14d. The weak amplitude areas above and below the centre are caused by the small offsets in the centre of the cross-spread, which have smaller Fresnel zones than the long offsets. True-amplitude migration would compensate for this effect.

## ***Discussion***

This paper provides a framework for prestack processing of data acquired with orthogonal geometry. Quite a few prestack processes can be improved by selecting the most suitable input gather for that process. However, implementation of the ideas requires further work, including some software development. Testing of the ideas is likely to lead to further insights and modifications to the proposed techniques.

In most discussions it has been assumed that in-line fold and cross-line fold are even numbers. Small modifications are necessary for odd values of in-line and cross-line fold.

It should be clear that a data set acquired with a multi-line roll geometry cannot benefit as much from the ideas in this paper as the regular one-line roll, which is standard in 3D symmetric sampling. With a multi-line roll, asymmetric cross-spreads are acquired, making it impossible to cover the whole survey area with (*SLI*, *RLI*) sized OVS gathers, because OVSs occurring in one cross-spread are missing in the next.

It is interesting to note that wide acquisition geometry is not essential to applying most techniques. OVS gathers may also be constructed from narrow geometries.

Most techniques can also be applied to other acquisition geometries using their unit cells as a basis for OVS gathers. In a slanted geometry the slanted spread can be subdivided in diamond-shaped subsets with dimensions again determined by source line interval and receiver line interval. However, the spatial discontinuities across OVS boundaries in a slanted geometry are larger than in the equivalent orthogonal geometry.

## **Conclusions**

Prestack processing of data acquired with orthogonal geometry or any other crossed-array technique is much more complicated than processing of data acquired with parallel geometry. In parallel geometry use can be made of common-offset gathers as MDSs, which extend across the whole survey area. In orthogonal geometry only pseudo-minimal data sets are available and these should be exploited for optimal prestack processing. The pMDSs can be constructed by taking offset-vector slots from corresponding positions in all cross-spreads of the geometry. The spatial discontinuities, which are inherent in the orthogonal geometry, will be thinly distributed across the survey area by these OVS gathers. Most processing ideas in this paper have not been put to the test yet. Before that can be done, some software development is necessary, although some ideas can be implemented with only minor modifications to existing software.

## **Acknowledgement**

Prestack time migration results shown in Figure 15 were produced with prototype software provided by Seismic Image Software Ltd.

## References

- Albertin, U., et al., 1999, Aspects of true amplitude migration: 69th Ann. Internat. Mtg., Soc. Expl. Geophys., Expanded Abstracts, Paper SPRO 11.2.
- Anstey, N., 1986, Whatever happened to ground roll?: *The Leading Edge*, **5**, no. 3, 40–45.
- Bleistein, N., 1987, On the imaging of reflectors in the earth: *Geophysics*, **52**, 931-942.
- Bloor, R., Albertin, U., Jaramillo, H., and Yingst, D., 1999, Equalised prestack depth migration: 69th Ann. Internat. Mtg., Soc. Expl. Geophys., Expanded Abstracts, Paper SPRO 11.3.
- Cary, P.W., 1999, Common-offset-vector gathers: an alternative to cross-spreads for wide-azimuth 3-D surveys: 69th Ann. Internat. Mtg., Soc. Expl. Geophys., Expanded Abstracts, Paper SPRO P1.6.
- Collins, C.L., 1997, Imaging in 3-D DMO, part I: Geometrical optics model: *Geophysics*, **62**, 211-224.
- Cox, M., 1999, Static corrections for seismic reflection surveys: *Soc. Expl. Geophys.*
- Harris, C.C., Marcoux, M.O., and Bickel, S.H., 1998, MITAS, migration input trace aperture selection: 68th Ann. Internat. Mtg., Soc. Expl. Geophys., Expanded Abstracts, Paper SP 10.7.
- Hill, S., Shultz, M., and Brewer, J., 1999, Acquisition footprint and fold-of-stack plots: *The Leading Edge*, **18**, 686-695.
- Jack, E., 1999, The future is random: archiving seismic data to random access media: 69th Ann. Internat. Mtg., Soc. Expl. Geophys., Expanded Abstracts, Paper SACQ 3.8.
- Miao, X., and Cheadle, S., 1998, Noise attenuation with wavelet transform: 68th Ann. Internat. Mtg., Soc. Expl. Geophys., Expanded Abstracts, Paper SP 1.1.
- Ongkiehong, L., and Askin, H., 1988, Towards the universal seismic acquisition technique: *First Break*, **5**, 435–439.
- Padhi, T., and Holley, T. K., 1997, Wide azimuths—why not?: *The Leading Edge*, **16**, 175–177.
- Rousseau, V., Nicoletis, L., Svay-Lucas, J., and Rabotoarisoa, H., 2000, 3D true amplitude migration by regularization in angle domain: paper submitted for 62nd Mtg., Eur. Assoc. Geosc. and Eng., Extended Abstracts.
- Tura, A., Hanitzsch, C., and Calandra, H., 1998, 3-D AVO migration / inversion of field data: *The Leading Edge*, **17**, 1578-1583.
- Tygel, M., Schleicher, J., Hubral, P. and Hanitzsch, C., 1993, Multiple weights in diffraction stack migration: *Geophysics*, **58**, 1820-1830.
- Vermeer, G. J. O., 1990, Seismic wavefield sampling: *Soc. Expl. Geophys.*
- , 1994, 3-D symmetric sampling: 64th Ann. Internat. Mtg., Soc. Expl. Geophys., Expanded Abstracts, 906–909.
- , 1998a, 3-D symmetric sampling: *Geophysics*, **63**, 1629-1647.
- , 1998b, 3-D symmetric sampling in theory and practice: *The Leading Edge*, **17**, 1514-1519.
- , 1998c, Creating image gathers in the absence of proper common-offset gathers: *Exploration Geophysics*, **29**, 636-642.
- Vermeer, G.J.O., den Rooijen, H.P.G.M, and Douma, J., 1995, DMO in arbitrary 3-D geometries: 65th Ann. Internat. Mtg., Soc. Expl. Geophys., Expanded Abstracts, 1445-1448.

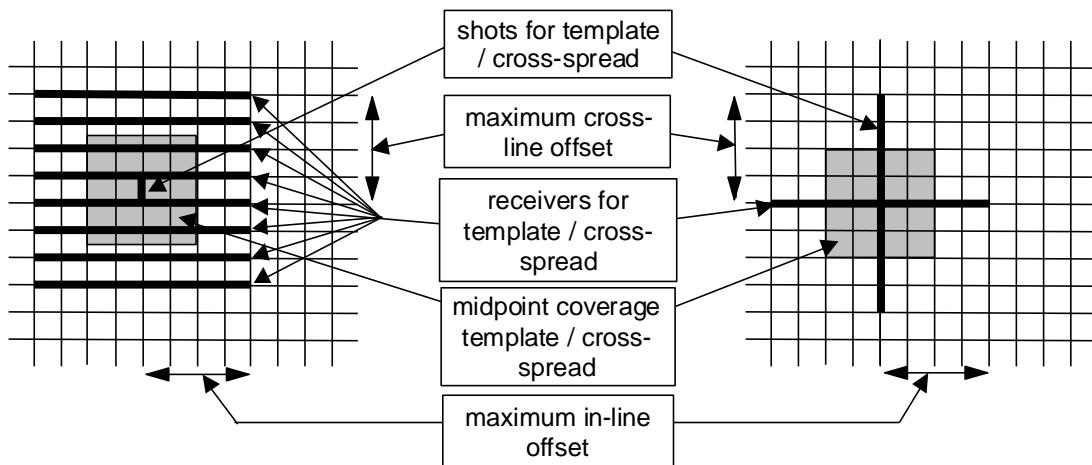


FIG. 1. The same orthogonal geometry with template (left) and with cross-spread (right). Horizontal lines are receiver lines; vertical lines are source lines. The template represents the way in which the data is acquired in the field; in this case there are 8 receiver lines with a number of shots in the centre of the template. The cross-spread gathers all data for receivers that have listened to a range of shots along the same source line.

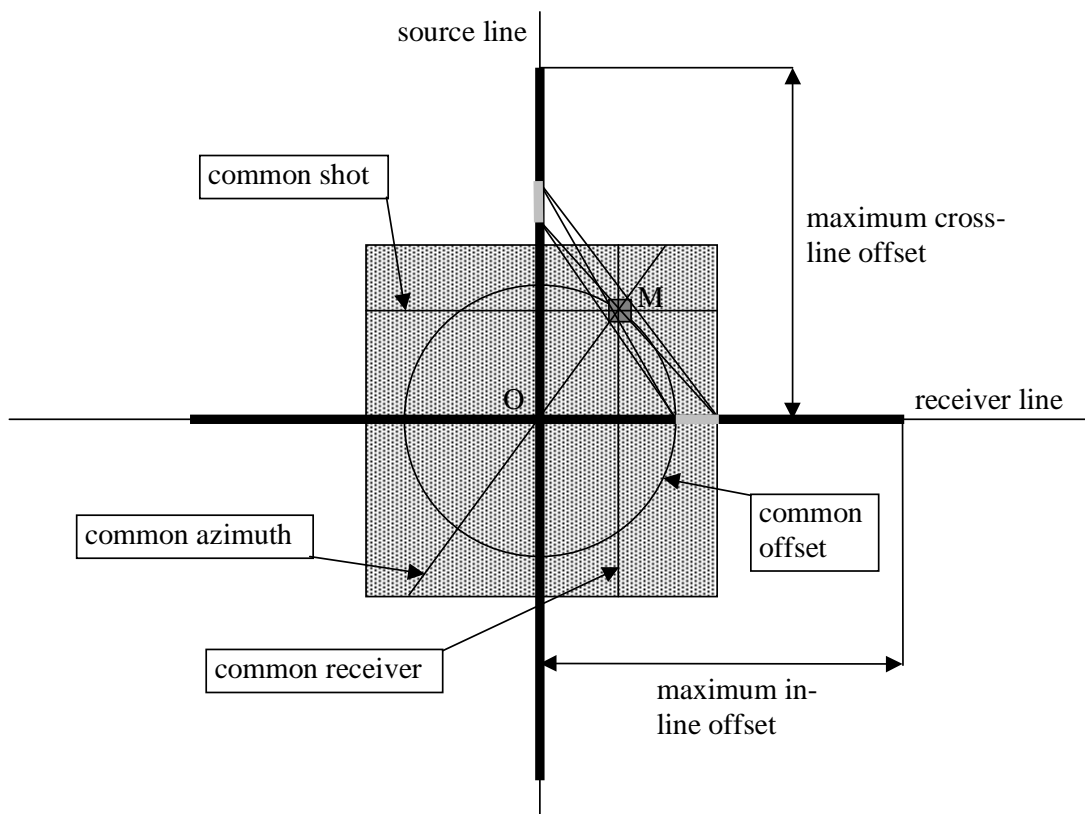


FIG. 2. Properties of cross-spread. The half-offset of a trace at  $M$  equals the distance to the center  $O$  of the cross-spread (i.e., traces with same offset lie on a circle). All traces close to  $M$  correspond to neighbouring shots on the source line and to neighbouring receivers on the receiver line.

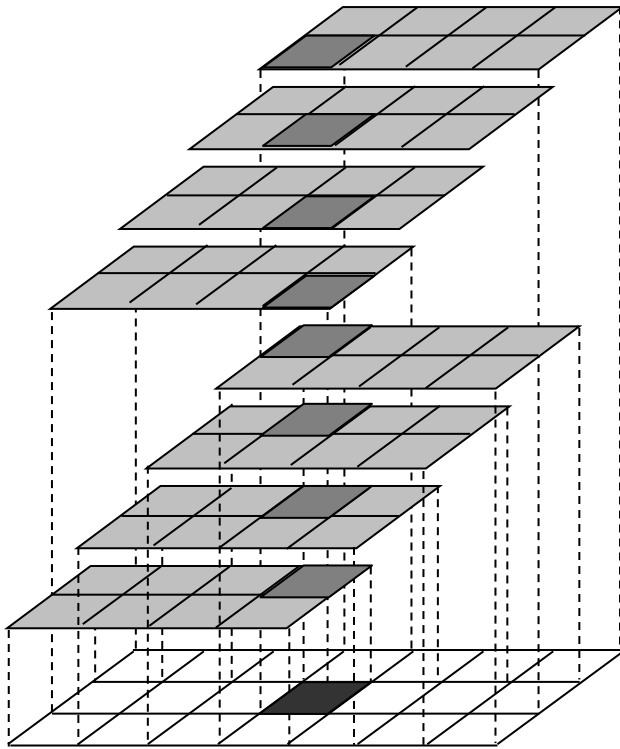


FIG. 3. Fold-of-coverage can be found by counting number of overlapping cross-spreads. In this case in-line fold is four and cross-line fold is two: there are eight overlapping cross-spreads in each point.

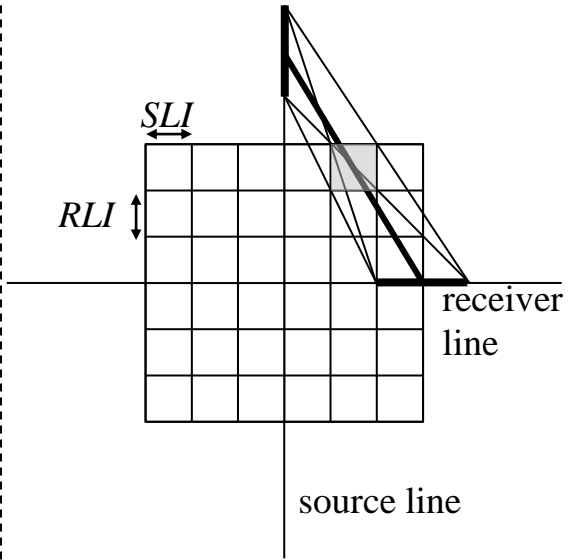


FIG. 4. Unit-cell-sized offset-vector slot in cross-spread of 36-fold geometry. Heavy lines along source line and receiver line indicate range of shots and receivers contributing to OVS. Heavy line through middle of OVS indicates average offset and average shot/receiver azimuth.

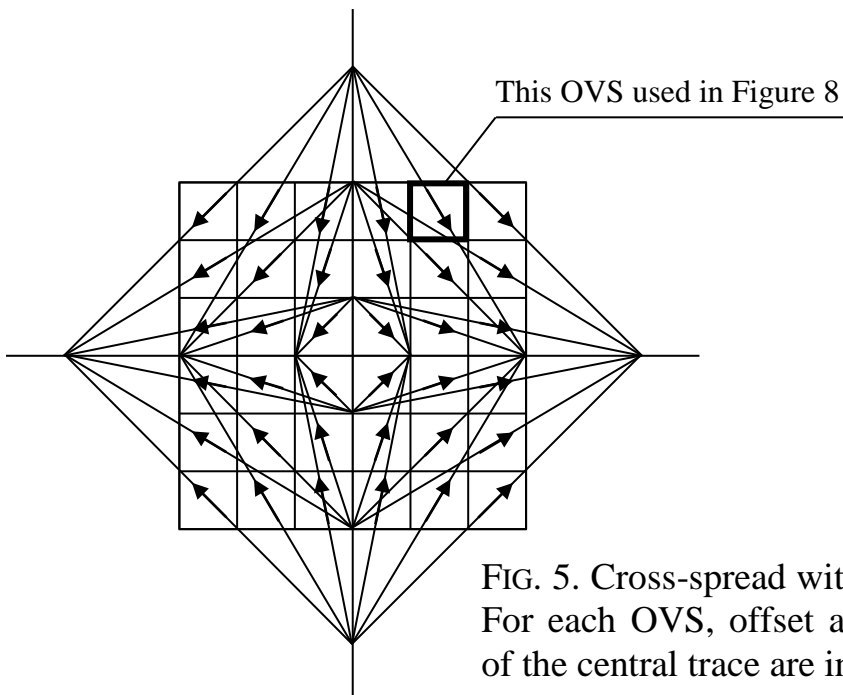


FIG. 5. Cross-spread with its OVSs. For each OVS, offset and azimuth of the central trace are indicated.

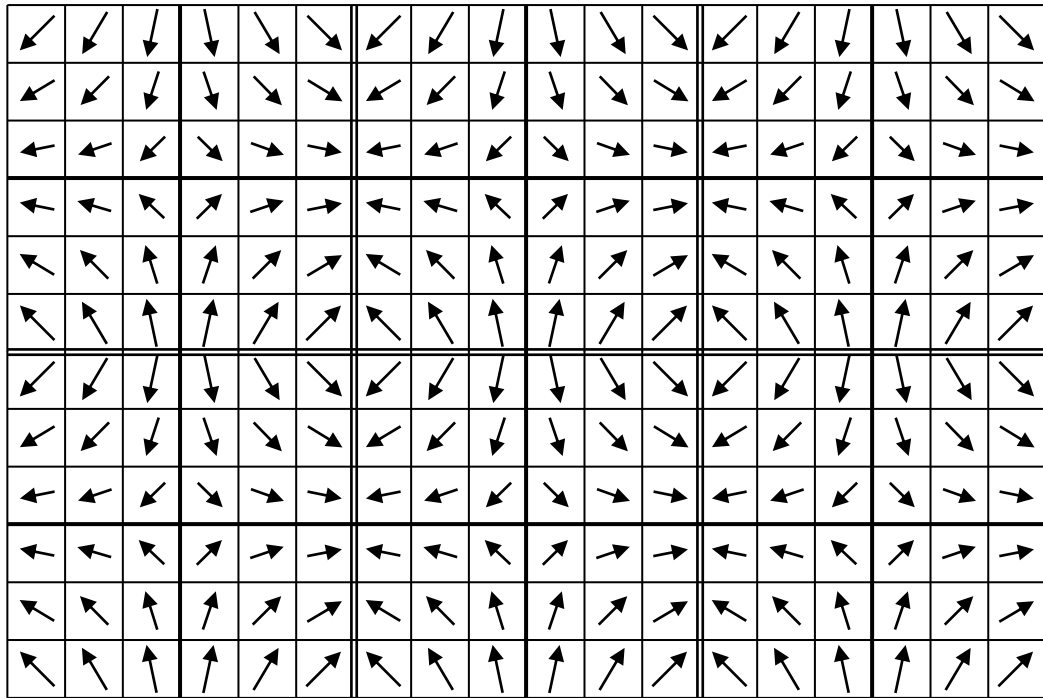


FIG. 6. Tiling with (six) adjacent cross-spreads. Spatial continuity exists inside the cross-spreads, but large discontinuities occur across the edges of each cross-spread, in particular in the corners. From the corners to the axes of the cross-spreads, the discontinuities decrease.

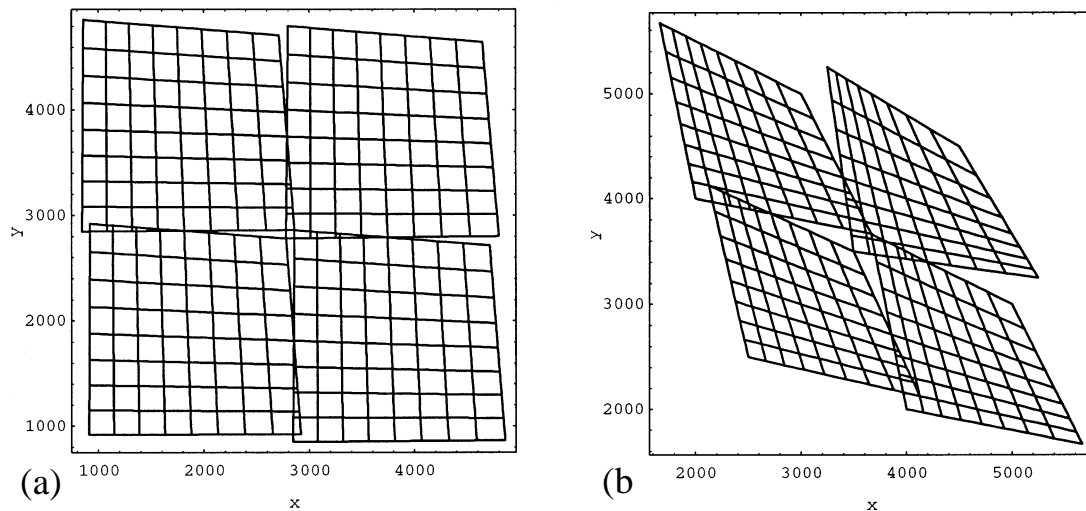


FIG. 7. Illumination of  $15^\circ$  (a) and  $45^\circ$  (b) dipping reflectors by four adjacent cross-spreads. Each cross-spread illuminates a continuous area of the reflector, but between cross-spreads gaps and overlaps exist.

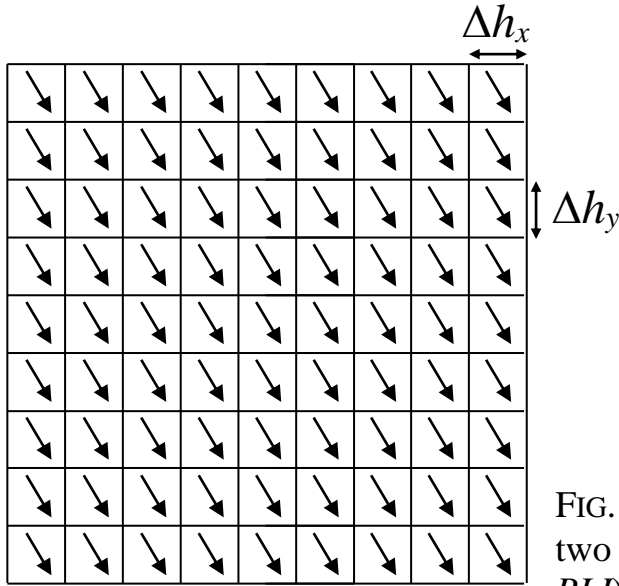


FIG. 8. Pseudo-minimal data set constructed from offset-vector slots. In this case, the generating OVS is the upper central OVS in the first quadrant of all cross-spreads (cf. Figure 5). In this OVS gather the spatial discontinuities are spread thinly across the whole survey area.

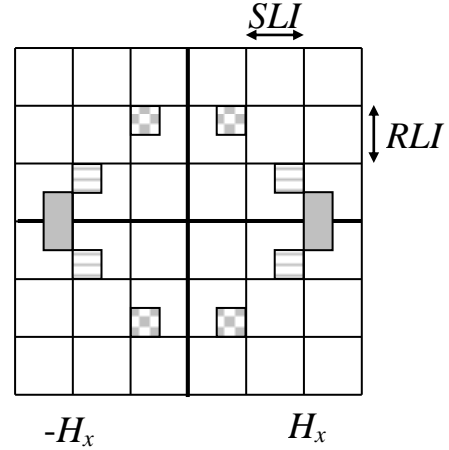


FIG. 9. Special case OVSs. Together, the two rectangular OVSs (dimension  $\frac{1}{2} SLI \times RLI$ ) can be used to construct an OVS gather with small spatial discontinuity between the OVSs. Together, the four chequered squares (dimension  $\frac{1}{2} SLI \times \frac{1}{2} RLI$ ) may be used to construct an OVS gather in case azimuth does not play a significant role. The locations of these OVSs may be selected anywhere inside the cross-spread, provided the pairs or quartets occupy mirrored positions. The eight small squares may be assigned the same mute time to achieve constant fold.

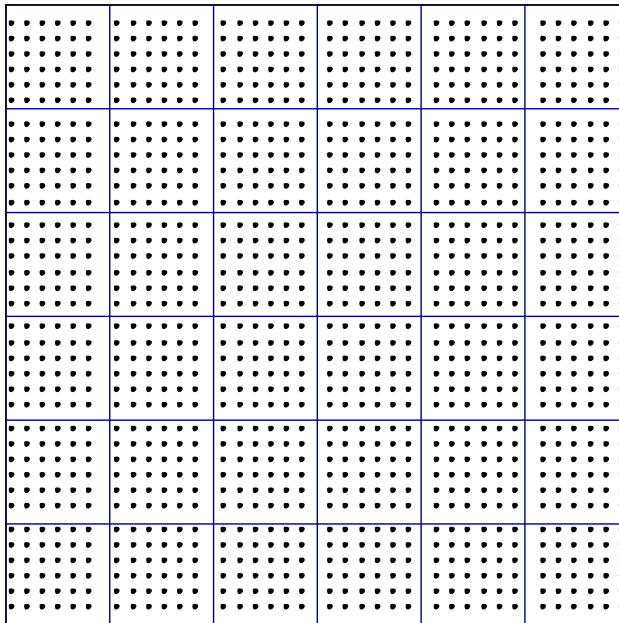


FIG. 10. Unit cell with offset distribution in each bin for a 36-fold geometry. Each square represents a bin. The 36 traces in each bin correspond to 36 different cross-spreads. Each bin has its own  $(h_x, h_y)$ -coordinate system centred in the bin. Nearest neighbours inside the bin have at least one different acquisition line.

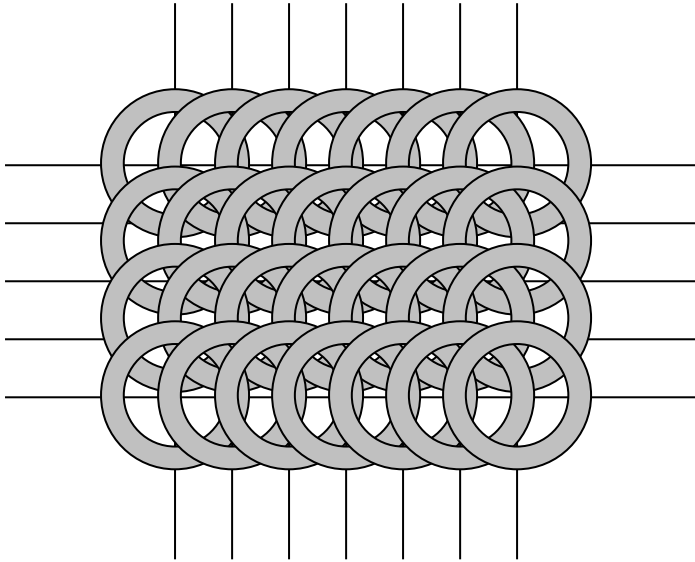


FIG. 11. Offset-range gather in orthogonal geometry. Each ring represents traces in midpoint domain with a narrow range of absolute offsets.

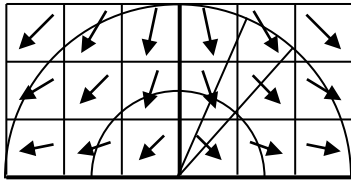


FIG. 12. Basic unit for AvO and amplitude versus azimuth analysis. All OVSs corresponding to the same unit-cell sized part of the survey area are displayed next to each other for further analysis. OVSs with opposite azimuth have been stacked together. Amplitudes for the same offset can be averaged along rings with a constant absolute offset range. Repeating this for all relevant positions in the survey area allows to analyse the spatial variation of the AvO effect. Azimuth-dependent effects can be analysed using pie-slice shaped areas, which contain data with the same azimuth range.

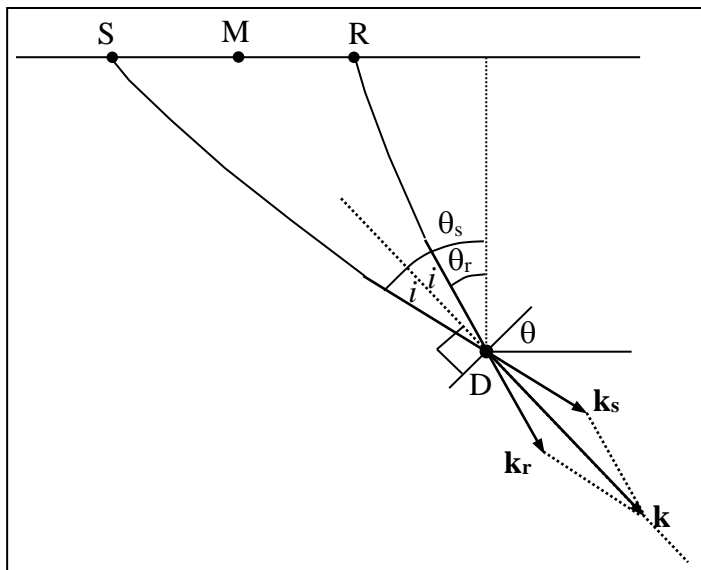


FIG. 13. Illumination of diffractor D by shot/receiver pair S/R. The directions of the raypaths at D determine the shot and receiver wavenumber components of total wavenumber  $\mathbf{k}$ . SD and RD are also the reflection raypaths for a reflector through D with dip angle  $\theta = (\theta_s + \theta_r)/2$ . The raypaths make an angle  $i = (\theta_s - \theta_r)/2$  with  $\mathbf{k}$ .

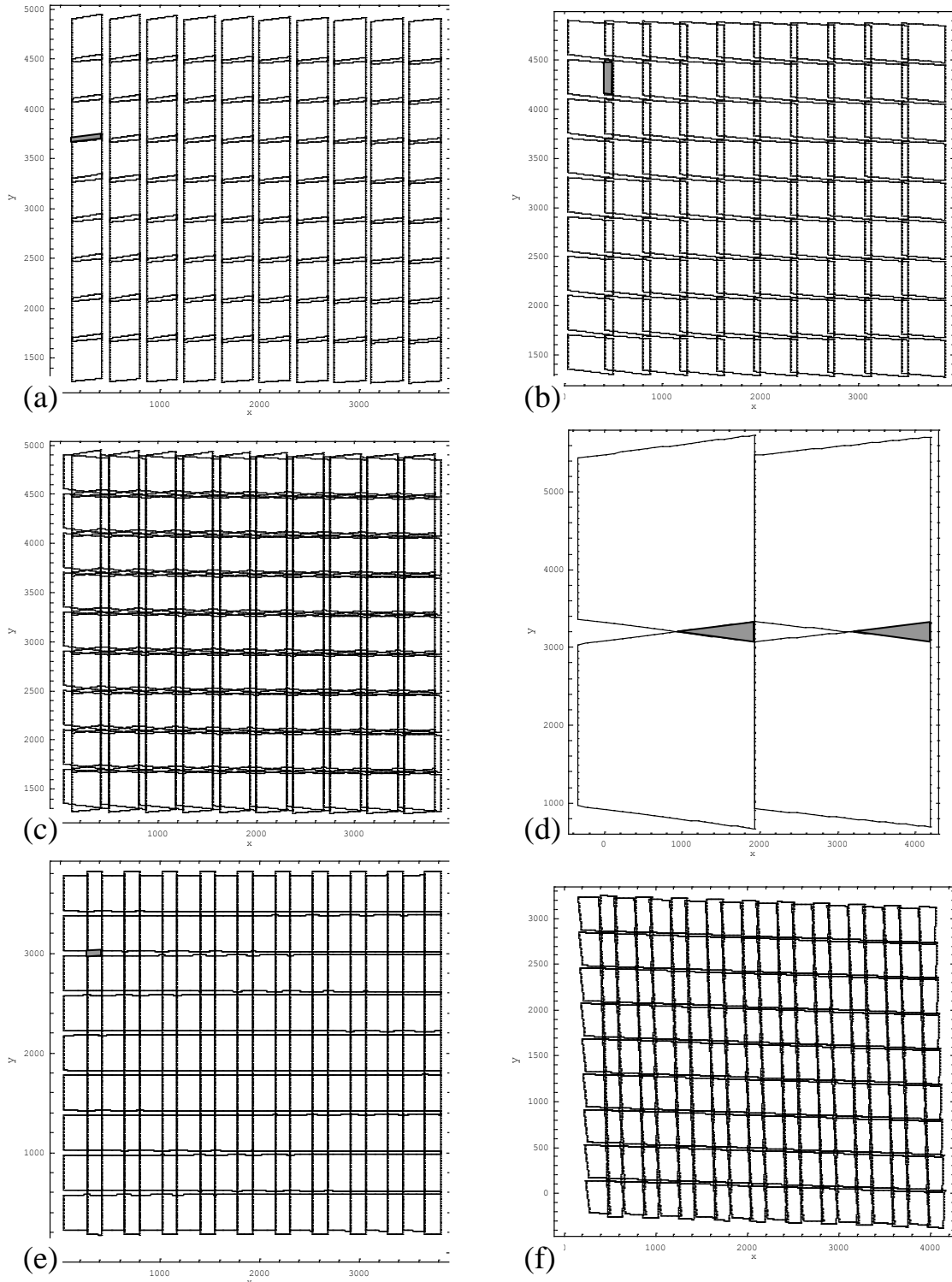


FIG. 14. Illumination of east dipping reflector by OVS gathers. (a) OVS of upper right corner in cross-spread. (b) OVS of lower left corner. (c) Superposition of (a) and (b). (d) Adjacent cross-spreads. (e) Rectangles from far end of receiver line (cf. Figure 9). (f) As (e) with dip azimuth of  $135^\circ$ . Grey areas indicate overlapping illumination areas.

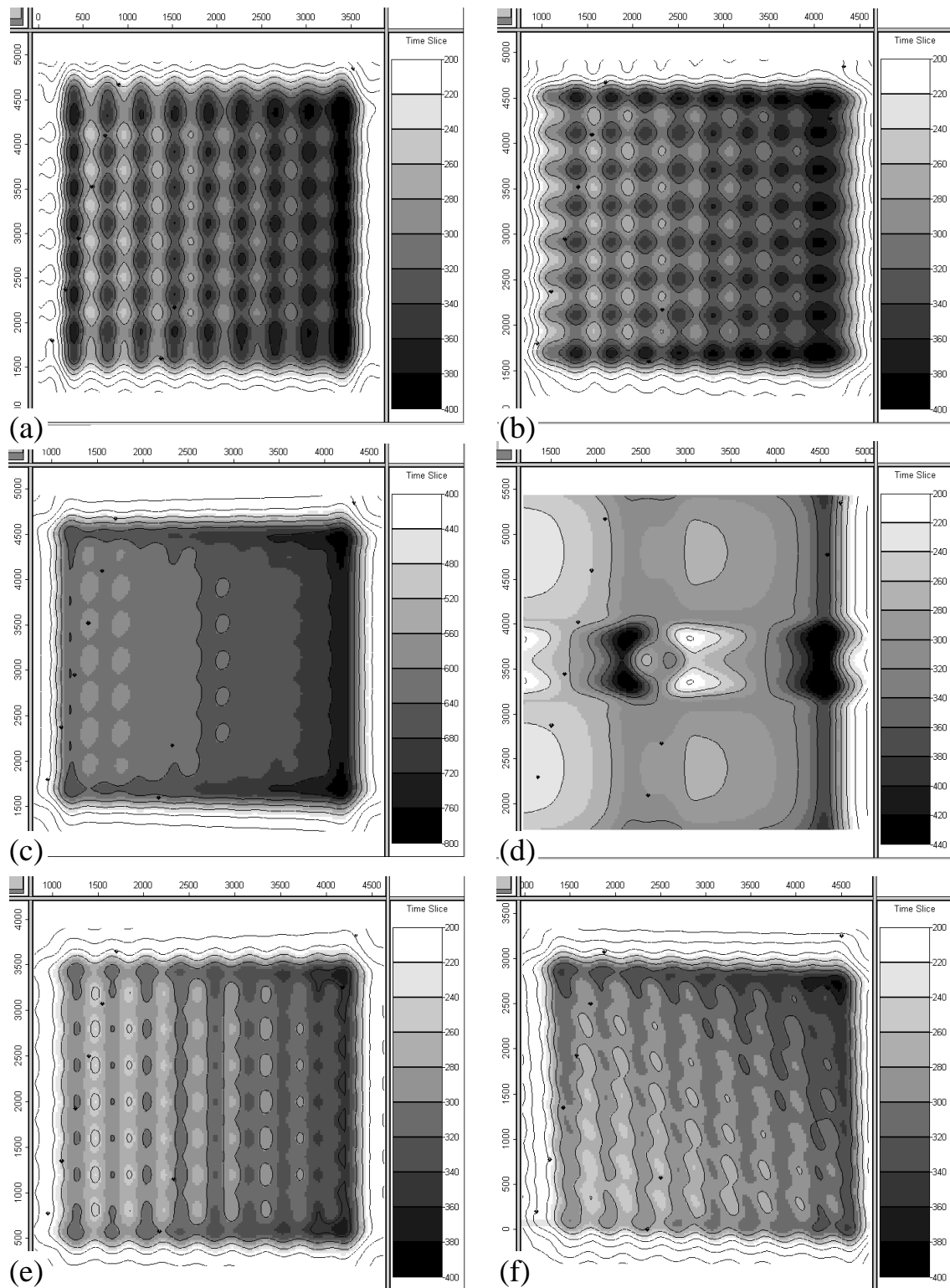


FIG. 15. Imaging of east dipping reflector by OVS gathers. Each figure shows a horizon slice for the corresponding situation in Figure 14. Contour interval in all slices is the same, except in Figure 15c, where it is twice as large as in the other displays.